

Transport and magnetic properties of $\text{La}_{1-x}\text{Ca}_x\text{VO}_3$

K. Maiti, N. Y. Vasanthacharya and D. D. Sarma*

Solid State and Structural Chemistry Unit, Indian Institute of Science, Bangalore 560 012, INDIA

(October 13, 2018)

Abstract

We report the temperature dependence of transport and magnetic properties of $\text{La}_{1-x}\text{Ca}_x\text{VO}_3$ for $x = 0.0, 0.1, 0.2, 0.3, 0.4$ and 0.5 . The system exhibits an insulator-to-metal transition concomitant with an antiferromagnetic-to-paramagnetic transition near $x = 0.2$ with increasing substitution. Disorder effects are found to influence the low temperature transport properties of both insulating and metallic compositions near the critical concentration. At higher temperatures, the resistivity of the metallic samples is found to exhibit either a $T^{1.5}$ or a T^2 dependence depending on the composition. The molar susceptibility for the metallic samples indicate substantial enhancements due to electron correlation.

PACS Numbers: 71.30.+h, 71.27.+a, 75.20.Hr, 75.30.Cr

I. INTRODUCTION

The study of metal-insulator transition in early transition metal (Ti and V) oxides has attracted a lot of attention in recent times [1–8]. Most of these oxides have the perovskite structure which allows for doping of charge carriers by chemical heterovalent substitutions over a wide range of compositions without breaking the structural network. Moreover, this basic structure type makes it possible to tune various structural parameters, such as the bond angles and bond lengths, which directly affect the bandwidth by altering the intra- and inter-cluster hopping interactions. Thus, it becomes possible to investigate metal-insulator transitions as a function of charge carrier tuning as well as bandwidth (or correlation effects) control.

Two such series of compounds that are related to the present work are $\text{La}_{1-x}\text{Sr}_x\text{VO}_3$ and $\text{Y}_{1-x}\text{Ca}_x\text{VO}_3$, which have been recently studied for several values of x [2,3,6]. LaVO_3 is an antiferromagnetic insulator with Néel temperature around 140 K [9], with a distorted perovskite structure [10–15]. Optical conductivity measurement [4] suggests the charge excitation gap (the Mott-Hubbard gap) to be about 1.1 eV. Substitution of trivalent La with divalent Sr effectively leads to the doping of holes into the system, thereby driving it to a metallic phase at about 22% hole doping [16], a value very near to the percolation threshold ($x \sim 0.26$). The system remains antiferromagnetic throughout the insulating regime ($x \leq 0.2$) and shows paramagnetic susceptibility in the metallic phase [17]. The insulator to metal transition in this system has been believed to be driven by Anderson localization [3,18]. Sr substitution in this system drives the system towards the ideal cubic perovskite structure which is the structure of the end member SrVO_3 . YVO_3 is also an antiferromagnetic insulator with orthorhombically distorted perovskite structure [19]. Here the V-O-V bond angle is lower than that of LaVO_3 leading to a decreased bandwidth in YVO_3 . With the substitution of Y^{3+} by Ca^{2+} it transforms to a metallic phase, but the minimum amount of hole doping needed to get the metallic phase is very large ($x \sim 0.5$) compared to the case of $\text{La}_{1-x}\text{Sr}_x\text{VO}_3$ ($x \sim 0.22$). This large value of x in YVO_3 rules out

the possibility of percolation to be one explanation for the MI transition in this system. One possible reason for this large value for the critical concentration might be the smaller band width in YVO_3 compared to LaVO_3 discussed above. This suggests that changing electron correlation effects also play an important role in these doping dependent MI transitions.

We study the transport and magnetic properties of LaVO_3 and its Ca substituted compositions, $\text{La}_{1-x}\text{Ca}_x\text{VO}_3$ for various values of x . This system is different from $\text{La}_{1-x}\text{Sr}_x\text{VO}_3$ since the effective ionic radius Ca^{2+} (1.34 Å) is very close to that of La^{3+} (1.36 Å), in contrast to that of Sr^{2+} (1.44 Å) [20]. The crystal structures of the two end members LaVO_3 and CaVO_3 are both distorted perovskite type [2,10–15,21], whereas SrVO_3 is cubic [22]. Thus, unlike Sr^{2+} substitution, Ca^{2+} substitution in LaVO_3 dopes hole states without much change in structural parameters. In view of this, it is reasonable to expect that the changes in the transport and magnetic properties in $\text{La}_{1-x}\text{Ca}_x\text{VO}_3$ are more controlled by the tuning of the doping level with comparatively less influence from the changes in the correlation effects, in contrast to the previously studied $\text{La}_{1-x}\text{Sr}_x\text{VO}_3$ and $\text{Y}_{1-x}\text{Ca}_x\text{VO}_3$.

II. EXPERIMENTAL

The samples of $\text{La}_{1-x}\text{Ca}_x\text{VO}_3$ ($x = 0.0, 0.1, 0.2, 0.3, 0.4$ and 0.5) have been prepared by taking stoichiometric amounts of predried La_2O_3 , CaCO_3 and V_2O_5 in appropriate proportions. The components have been ground together and heated at 600°C and then 800°C for 24 hours each. Then the obtained mixture have been reground and reduced at 800°C for 24 hours in hydrogen atmosphere. Finally, the black color powder obtained has been ground and pelletized, and melted in a dc arc furnace in inert gas atmosphere. All the samples have been characterized by x-ray powder diffraction (XRD) pattern obtained from a JEOL-8P x-ray diffractometer using $\text{Cu K}\alpha$ radiation. XRD patterns show single phases for all the compositions. The structure remains the same, in the whole composition range prepared.

It is well known that there is always some amount of oxygen nonstoichiometry in these oxides [23–25]. We have estimated the exact oxygen content in each of the samples by

heating the samples at 500° C for about 72 hours in flowing oxygen, thereby converting all V ions to the highest oxidation state of V⁵⁺. By monitoring the weight gain in this process, we estimate that La_{1-x}Ca_xVO_{3+δ} samples formed with δ = 0.04, 0.03, 0.04, 0.01, -0.01 and 0.0 for x = 0.0, 0.1, 0.2, 0.3, 0.4 and 0.5 respectively. Thus it appears that there are some doped hole states arising from slightly nonstoichiometric compositions in addition to those introduced by heterovalent substitution of La³⁺ by Ca²⁺ in these samples, particularly for the samples with small values of x. As will be shown later in the text, such oxygen nonstoichiometry influences the low temperature transport properties of these samples especially within the insulating regime.

The resistivity measurements have been carried out using a dc four probe resistivity set up following Van der Pauw's method. The dc magnetic susceptibility measurements have been performed in the temperature range 20-300 K using a Lewis coil force magnetometer at a field of 5 kOe.

III. RESULTS AND DISCUSSION

We show the resistivity (ρ) of LaVO₃ as a function of temperature (T) in Fig. 1. The result clearly suggests an insulating behaviour for this compound. However the transport does not follow a single activated dependence as illustrated in the inset where we show the dependence of resistivity (ρ) on the temperature (T) in an $\ln \rho$ vs $1/T$ plot. The inset suggests a simple activated behavior at the high temperature regime, while there is a considerable deviation for $T < 120$ K (i.e. $1000/T > 8.5$). In this low temperature regime, the resistivity appears to be best described by the variable range hopping mechanism [16], as illustrated in the inset by the linear dependence of $\ln \rho$ on $1/T^{1/4}$. Combining these two behaviors, we find that the experimental transport data is well described over the entire temperature range in terms of simultaneous contributions to the conductivity (σ) both by an activated process and by variable range hopping (VRH) in the form :

$$\sigma = \sigma_{01} \exp\left[-\frac{E_g}{2K_B T}\right] + \sigma_{02} \exp\left[-\frac{T_0}{T^{1/4}}\right]$$

The resulting best fit is shown by a solid line through the data points in the main figure over the entire temperature range. From the fitting we obtain the value of the gap (E_g) to be about 0.12 eV. It is to be noted here that this estimate of the transport gap is about one order of magnitude smaller than the intrinsic Mott-Hubbard gap (1.1 eV) in LaVO_3 estimated from optical spectroscopy [4]. Thus we believe that the smaller gap arises from doping of hole states above the top of the valence band due to the inevitable presence of oxygen nonstoichiometry even in the undoped sample as already pointed out in the experimental section. This smaller gap is dominant for the transport properties at room temperature and below, since charge excitations across the large intrinsic Mott-Hubbard gap are suppressed at these temperatures. The small contribution from VRH to the conduction process at the lowest temperature suggests the presence of low but finite density of states (DOS) localized due to disorder effects [3] at the Fermi energy. We discuss further these aspects later in the text.

The resistance of the smallest substituted composition $\text{La}_{0.9}\text{Ca}_{0.1}\text{VO}_3$ is plotted as a function of temperature in Fig. 2. The diverging resistivity with decreasing temperature suggests a non-metallic ground state of this sample in spite of 0.1 hole doping in every formula unit. In order to understand the nature of the non-metallic state in this case, we plot $\ln \rho$ as a function of $1/T$ in the inset. The high temperature (approximately $T > 110$ K or $1000/T < 9$) end of this plot shows an activated behavior as suggested by the straight line through the data in the inset; however, the resistivity plot deviates markedly at lower temperatures. In the inset of Fig. 2, it is seen that the logarithm of resistivity is linear in $1/T^{1/4}$ over a wide range of temperatures. These observations suggest that the transport properties of $\text{La}_{0.9}\text{Ca}_{0.1}\text{VO}_3$ is dominated by variable range hopping [16] for $T < 110$ K, while an activated process contributes significantly for $T > 110$ K. In this case also the experimental data can be accurately described under the assumption that the total conduction process

is contributed simultaneously by variable range hopping and an activated process over the entire temperature range; this is illustrated by the solid line through the data in the main frame in Fig. 2, representing the best fit. This fit yields an estimate of the gap in the activated charge transport process to be 0.10 eV. In all this respect, the transport behavior of $\text{La}_{0.9}\text{Ca}_{0.1}\text{VO}_3$ is very similar to that of LaVO_3 , including very similar gaps in both cases. Quantitatively, however, the VRH appears to dominate over a more extensive temperature range in the case of the Ca doped sample compared to LaVO_3 , as can be seen comparing the plots in the insets of Figs. 1 and 2. This suggests that hole doped states arising from Ca substitution in the place of La leads to hole doped states in a similar energy range as that introduced by oxygen nonstoichiometry in the parent compound. Larger extent of hole doping in the former however leads to higher DOS at E_F leading to a manifestation of VRH more extensively, though the DOS at E_F in both cases are localized due to disorder effects.

Doping with $x \geq 0.2$ in $\text{La}_{1-x}\text{Ca}_x\text{VO}_3$ drives the system into a metallic state. This is illustrated in Fig. 3 where we plot the resistivity as a function of temperature for samples with $x = 0.2, 0.3, 0.4$ and 0.5 . The plots clearly indicate metallic behaviour of these compositions, except for an upturn of resistivity with decreasing temperature below 100 K for $x = 0.2$ and 0.3 samples exhibiting a negative temperature coefficient of resistivity (TCR). Similar behaviour has also been reported for $\text{La}_{1-x}\text{Sr}_x\text{VO}_3$ [4]. In spite of this increasing resistivity with decreasing temperature below 100 K, the samples appear to have a finite $\rho(T \rightarrow 0 \text{ K})$. This is better illustrated in the inset where we plot the conductivities of these two samples as a function of $T^{1/2}$ in the low temperature (negative TCR) region. These two plots suggest that the low temperature conductivity $\sigma(T)$ is well described by the relationship $\sigma(T) = \sigma(0) + \beta T^{1/2}$, where $\sigma(0)$ is the finite conductivity at $T = 0$ and the second term describes a square-root behaviour. Such a temperature dependence of conductance is well known in disordered metals in presence of strong electron-electron interaction effects [26,27]. It is indeed reasonable to expect that disorder will have some influence on the properties of such samples. After all, such substituted samples are intrinsically disordered due to the random substitution in the lattice. Moreover, various disorder effects must be the driving

force for the insulating state obtained with finite but small level of substitution ($x < 0.2$), since there cannot be a Mott-Hubbard insulator or a band insulator at arbitrary filling (or x). This view point is further substantiated by the variable range hopping exhibited by the insulating compositions. Thus, it is not surprising that the disorder effects manifest itself even in the metallic phase near the critical concentration in the form of a $T^{1/2}$ dependence of the conductivity at the low temperatures. Only deep into the metallic phase ($x \geq 0.4$) does it appear that the random potentials are sufficiently screened out by the metallic charge carriers and thus, there is no upturn of resistivity at the low temperatures for such compositions (see Fig. 3).

While normal metallic systems are expected to show a T^2 dependence of resistivity, recently it has been shown [4] that the resistivity of the closely related system $\text{La}_{1-x}\text{Sr}_x\text{VO}_3$ is well described by a $T^{1.5}$ dependence. This was attributed to strong spin fluctuation effects [28,29] with a Curie-Weiss-like susceptibility near the antiferromagnetic wave vector for these nearly antiferromagnetic metallic samples. We have explored whether a similar behaviour is also found in the present case. Thus, we plot the resistivity data as functions of $T^{1.5}$ and T^2 in Figs. 4a and 4b respectively for these metallic compositions leaving out the part of the resistivity data with negative TCR for $x = 0.2$ and 0.3 at the lowest temperatures. These results clearly reveal a systematic behaviour. For smaller values of x ($= 0.2$ and 0.3), the resistivities at higher temperatures ($T > 100$ K) are better described by the T^2 dependence and a $T^{1.5}$ dependence is clearly not consistent with the data. With increasing x ($=0.4$ and 0.5), however, $T^{1.5}$ dependence provides the best description for the experimental results with clear deviations from a T^2 behaviour. This appears to be a reversed trend compared to the case of $\text{La}_{1-x}\text{Sr}_x\text{VO}_3$ [4], where the $T^{1.5}$ behaviour was most dominant for small values of x close to the critical composition. While it is not clear at present if the physics of the Sr and Ca substituted LaVO_3 should be fundamentally different arising from the structural differences referred to in the introduction, it is hoped that single crystal data on both systems will resolve this issue in the future.

The temperature dependence of magnetic susceptibility of the insulating compositions,

LaVO_3 and $\text{La}_{0.9}\text{Ca}_{0.1}\text{VO}_3$ have been plotted in Fig. 5. In both cases, there is a maximum in the susceptibility, typical of an antiferromagnetic system; from these results, we obtain the Néel temperature for LaVO_3 to be around 125 K and that of $\text{La}_{0.9}\text{Ca}_{0.1}\text{VO}_3$ to be around 115 K. The further increase in susceptibility below T_N in the case of $\text{La}_{0.9}\text{Ca}_{0.1}\text{VO}_3$ may be due to the presence of localized isolated magnetic moments near the doped sites. The magnetic susceptibilities of the metallic compositions are shown in Fig. 6 for $x = 0.2, 0.3, 0.4$ and 0.5 . In every case the susceptibility is nearly independent of temperature at the higher temperature region with a distinct increase at the low temperatures. Such an increase in the magnetic susceptibility at low temperature is generally associated with the presence of localized magnetic impurities, while temperature independent component arises from Pauli-paramagnetism of the conduction electrons. Thus, we have analyzed the data in Fig. 6 in terms of these two contributions. These analysis yield Pauli paramagnetic susceptibilities (χ_{PP}) of $958, 836, 828$ and 728×10^{-3} emu/mole for $x = 0.2, 0.3, 0.4$ and 0.5 respectively. Thus, there is a monotonic decrease in susceptibility with x . Moreover, in every case, χ_{PP} appears to be enhanced by approximately a factor of two compared to the free electron value, suggesting the presence of correlation effects.

On the basis of the present results we summarize the evolution of the electronic structure in $\text{La}_{1-x}\text{Ca}_x\text{VO}_3$ with composition as depicted schematically in Fig. 7. Fig. 7a depicts the schematic single particle excitation spectra for both the occupied (lower Hubbard band, LHB) and unoccupied (upper Hubbard band, UHB) parts., separated by about 1.1 eV as suggested by the optical measurements [4]. Presence of oxygen non-stoichiometry in normally prepared composition, $\text{LaVO}_{3+\delta}$, introduces hole doped states primarily about 0.1 eV above the top of the LHB as shown in Fig 7b; this is evidenced by the activated transport with a characteristic gap of about 0.1 eV as shown in Fig 1. The low intensity tails of these states overlap the top of the LHB and thus, the Fermi energy, E_F , lies within a continuum of states. However, the low intensity continuum states in the vicinity of the E_F in Fig. 7b are localized due to disorder effects and thus lead to the VRH dominated $T^{1/4}$ dependence of conductivity at the lowest temperatures (see Fig. 1). Doping of Ca in place of La in

$\text{La}_{1-x}\text{Ca}_x\text{VO}_3$ with $x < 0.2$ (see Fig 7c) appears to dope hole states further in a similar energy range as in the case of $\text{LaVO}_{3+\delta}$ (Fig. 7b), thus, exhibiting similar temperature dependent resistivities in both the samples (compare Figs. 1 and 2). However, there are more continuum states at E_F in presence of 10% Ca doping ($x = 0.1$) compared to $\text{LaVO}_{3+\delta}$; thus, VRH in the Ca-doped case dominates over a wider temperature range. With further doping of Ca, the doped states become broader and more intense leading to a significant overlap with the LHB of the undoped compound and consequently lead to the metallic ground state for $x \geq 0.2$ (Fig. 7d). Within the metallic regime, the resistivity exhibits a T^2 behavior for the lower values (0.2 and 0.3) of x , changing over to a $T^{1.5}$ dependence for the higher values (0.4 and 0.5), with the Pauli paramagnetic susceptibilities exhibiting an enhancement of about two compared to the free-electron values.

IV. ACKNOWLEDGEMENTS

The authors thank G. Kotliar for useful discussions. KM acknowledges the Council of Scientific and Industrial Research, Government of India, for financial assistance.

REFERENCES

- * Also at Jawaharlal Nehru Centre for Advanced Scientific Research, Bangalore.
- [1] Y. Tokura, Y. Taguchi, Y. Okada, Y. Fujishima, T. Arima, K. Kumagai, and Y. Iye, Phys. Rev. Lett., **70**, 2126 (1993); K. Kumagai, T. Suzuki, Y. Taguchi, Y. Okada, Y. Fujishima, and Y. Tokura, Phys. Rev. B, **48**, 7636 (1993).
- [2] P. Dougier and P. Hagenmuller, J. Solid State Chem., **15**, 158 (1975).
- [3] N. F. Mott, M. Pepper, S. Pollitt, R. H. Wallis, and C. J. Adkins, Proc. R. Soc. (London), Ser. A, **345**, 169 (1975).
- [4] F. Inaba, T. Arima, T. Ishikawa, T. Katsufuji, and Y. Tokura, Phys. Rev. B, **52**, 2221 (1995).
- [5] P. Dougier, D. Deglane, and P. Hagenmuller, J. Solid State Chem., **19**, 135 (1976); H.C. Nguyen, and J.B. Goodenough, Phys. Rev. B, **52**, 8776 (1995).
- [6] M. Kasuya, Y. Tokura, T. Arima, H. Eisaki, and S. Uchida, Phys. Rev. B, **47**, 6197 (1993).
- [7] I.H. Inoue, I. Hase, Y. Aiura, A. Fujimori, Y. Haruyama, T. Moriyama, and Y. Nishihara, Phys. Rev. Lett., **74**, 2539 (1995).
- [8] D. B. McWhan, A. Menth, and J. P. Remeka, J. Phys. (paris) **32(C1)** 1079 (1971); S. A. Shivashankar and J. M. Honig, Phys. Rev. B, **28** 5695 (1983).
- [9] A. V. Mahajan, D. C. Johnston, D. R. Torgeson, and F. Borsa, Phys. Rev. B, **46**, 10966 (1992).
- [10] A. Wold and R. Ward, J. Amer. Chem. Soc., **76**, 1029 (1954).
- [11] H. L. Yakel, Acta Crystallogr., **8**, 394 (1955).
- [12] P. Dougier and A. Casalot, J. Solid State Chem., **2**, 396 (1970).

- [13] T. Shine-ike, T. Sakai, G. Adachi, and J. Shiokawa, *Mater. Res. Bull.*, **11**, 249 (1976).
- [14] V. G. Zubkov, G. V. Bazuev, P. A. Perelyaev, and G. P. Shveiken, *Fiz. Tverd. Tela* (Leningrad), **15**, 1610 (1973) [*Sov. Phys. Solid State*, **15**, 1078 (1973)].
- [15] P. Ganguly, Om Prakash, and C. N. R. Rao, *Phys. Status Solidi A*, **36**, 669 (1976).
- [16] N. F. Mott, *Metal - Insulator transitions*, (Taylor & Francis, London, 1994).
- [17] A. V. Mahajan, D. C. Johnston, D. R. Torgeson, and F. Borsa, *Phys. Rev. B*, **46**, 10973 (1992).
- [18] M. Sayer, R. Chen, R. Fletcher, and A. Mansingh, *J. Phys. C*, **8**, 2059 (1975).
- [19] M. Kasuya, Y. Tokura, T. Arima, H. Eisaki, and S. Uchida, *Phys. Rev. B*, **47**, 6197 (1993).
- [20] R. D. Shanon, *Acta Crystallographica*, **A32**, 751 (1976).
- [21] Fumitoshi Iga, and Yoshikazu Nishihara, *J. Phys. Soc. Jpn.*, **61**, 1867 (1992).
- [22] B. Reuter, and M. Wollnik, *Naturwissenschaften*, **50**, 569 (1963).
- [23] S.R. Barman, and D.D. Sarma, *Phys. Rev. B*, **49**, 16141 (1994).
- [24] A. Chainani, M. Mathew, D.D. Sarma, I. Das, and E.V. Sampathkumaran, *Physica B*, **186-188**, 995 (1993).
- [25] A. Chainani, M. Mathew, and D.D. Sarma, *Phys. Rev. B*, **48**, 14818 (1993).
- [26] C. Castellani, C. R. Natoli, and J. Raninger, *J. Phys. (Paris)*, **37(C4)**, 199 (1976).
- [27] B. L. Altshuler, A. G. Aronov, and P. A. Lee, *Phys. Rev. Lett.*, **44**, 1288 (1980).
- [28] T. Moriya, *Spin Fluctuations in Itinerant Electron Magnetism*, Springer (1985).
- [29] K. Ueda, *J. Phys. Soc. Jpn.*, **43**, 1497 (1977).

V. FIGURE CAPTIONS

Fig. 1 The resistivity of LaVO_3 as a function of the temperature. The open circles are the experimental data. The solid line shows the best fit assuming contributions from both variable range hopping and activated transport. The inset shows the $\ln \rho$ vs $1000/T$ and $\ln \rho$ vs $1/T^{1/4}$ plots.

Fig. 2 The resistivity of $\text{La}_{0.9}\text{Ca}_{0.1}\text{VO}_3$ as a function of the temperature. The open circles are the experimental data. The solid line is the best fit assuming contributions from both variable range hopping and activated transport. The inset shows the $\ln \rho$ vs $1000/T$ and $\ln \rho$ vs $1/T^{1/4}$ plots.

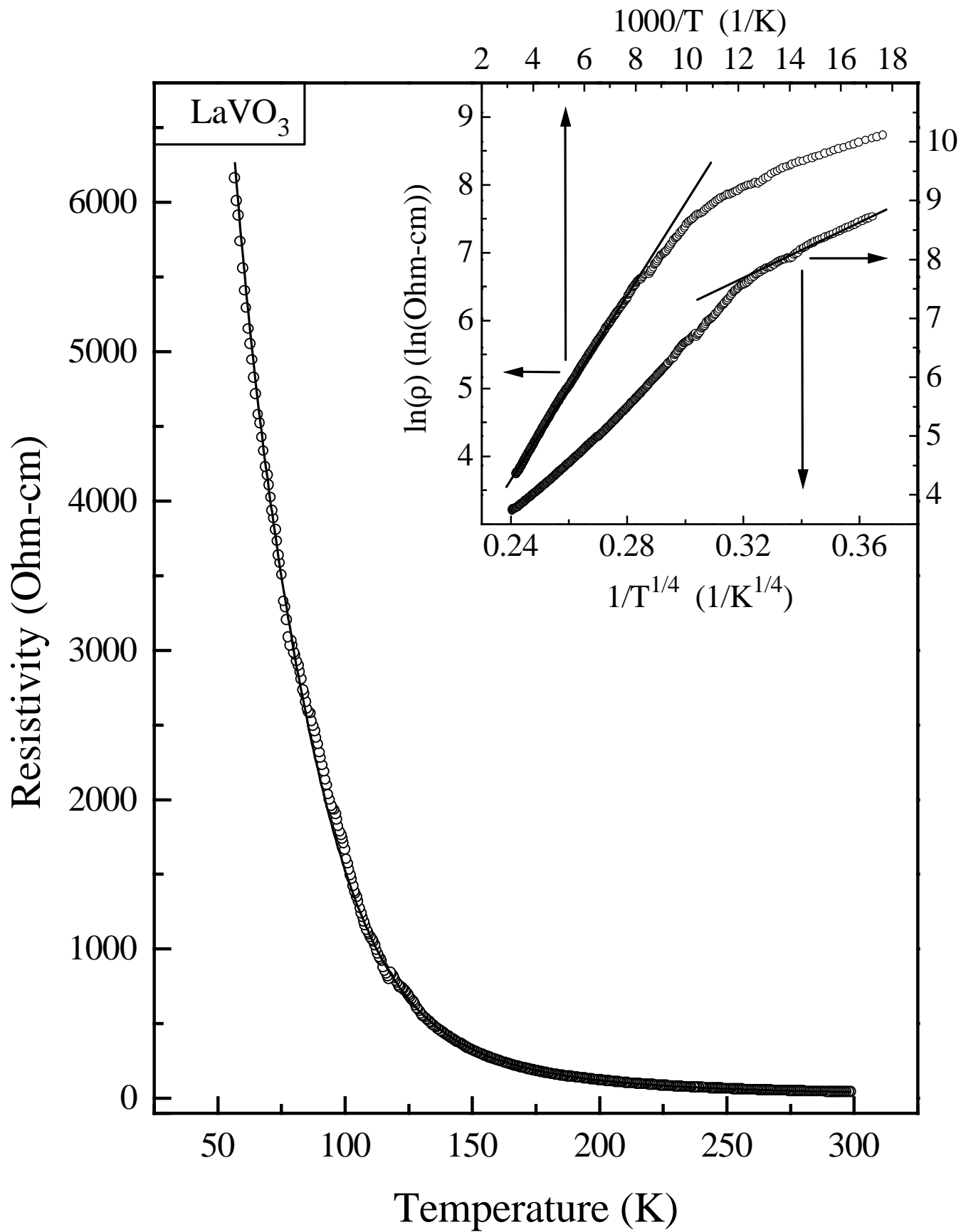
Fig. 3 The resistivity of $\text{La}_{1-x}\text{Ca}_x\text{VO}_3$ for $x = 0.2, 0.3, 0.4$ and 0.5 as a function of the temperature. The inset shows the $\ln \sigma$ vs $1/T^{1/2}$ plots for $x = 0.2$ and 0.3 in the low temperature region ($T < 100$ K).

Fig. 4 The resistivities of $\text{La}_{1-x}\text{Ca}_x\text{VO}_3$ for $x = 0.2, 0.3, 0.4$ and 0.5 as functions of (a) T^2 in the upper panel and (b) $T^{1.5}$ in the lower panel.

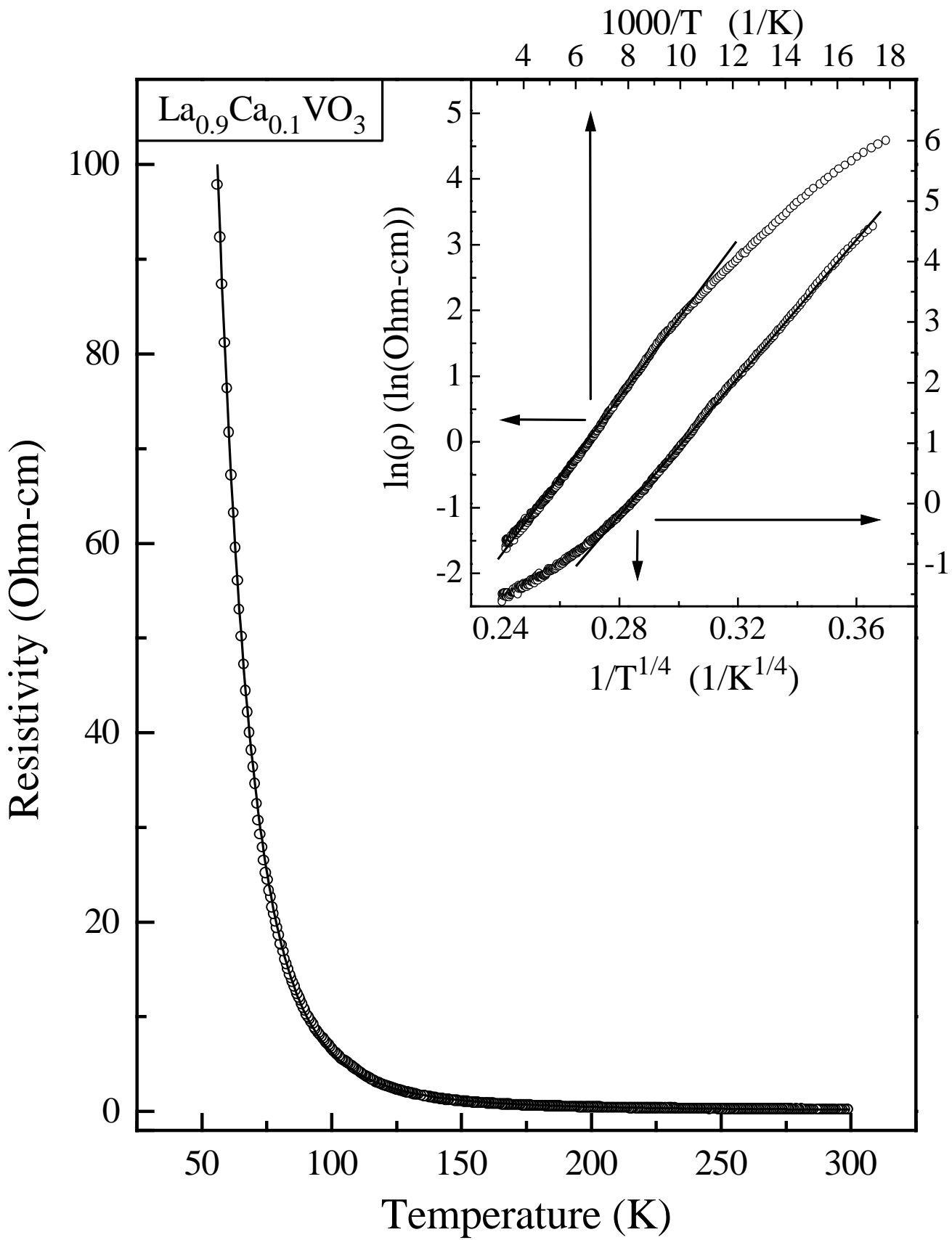
Fig. 5 The magnetic susceptibility of LaVO_3 (solid circles) and $\text{La}_{0.9}\text{Ca}_{0.1}\text{VO}_3$ (open circles).

Fig. 6 The magnetic susceptibility of $\text{La}_{1-x}\text{Ca}_x\text{VO}_3$ for $x = 0.2, 0.3, 0.4$ and 0.5 .

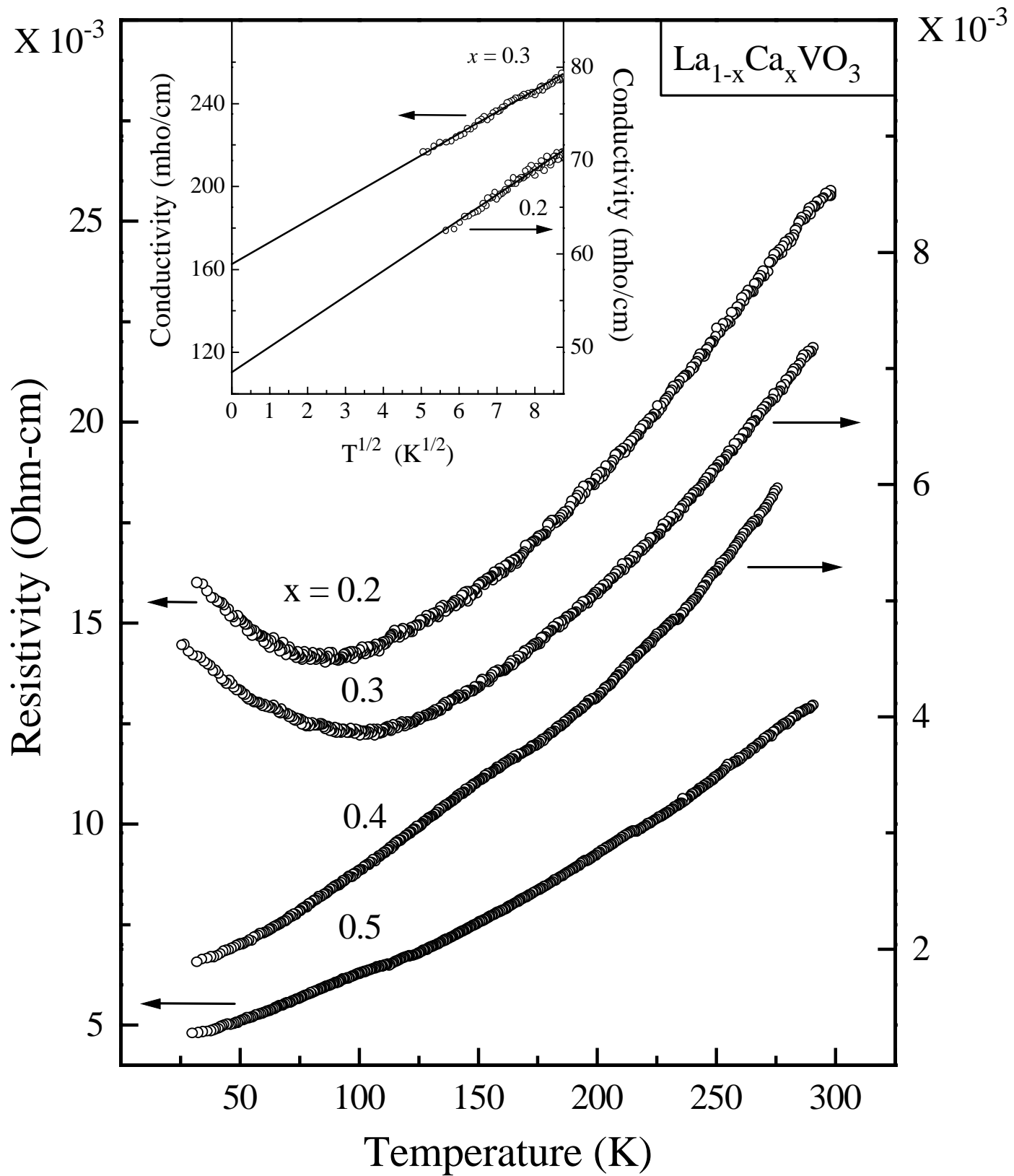
Fig. 7 The schematic energy diagrams for $\text{La}_{1-x}\text{Ca}_x\text{VO}_3$. (a) The case for $x = 0.0$, (b) $\text{LaVO}_{3+\delta}$, (c) $x < 0.2$, and (d) $x \geq 0.2$.



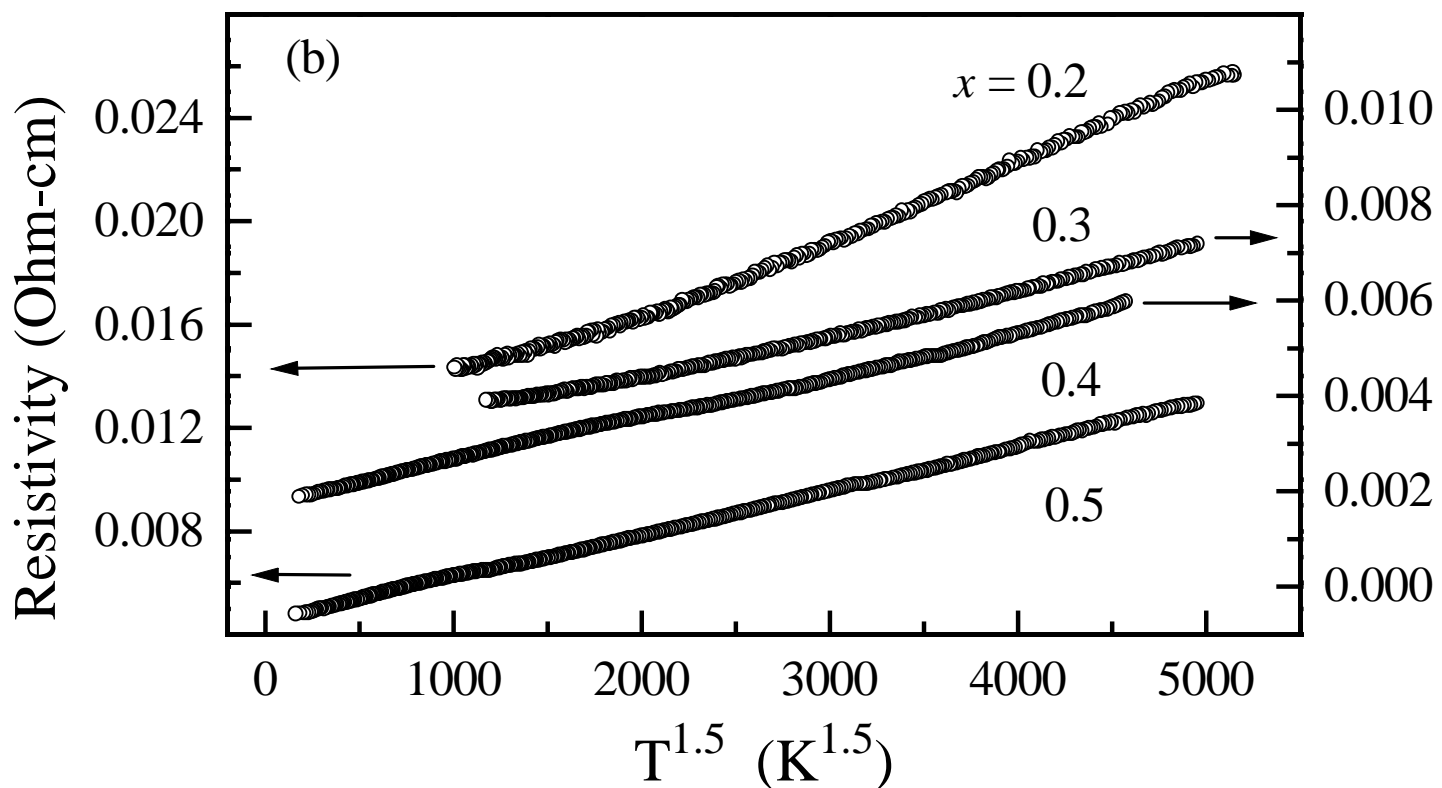
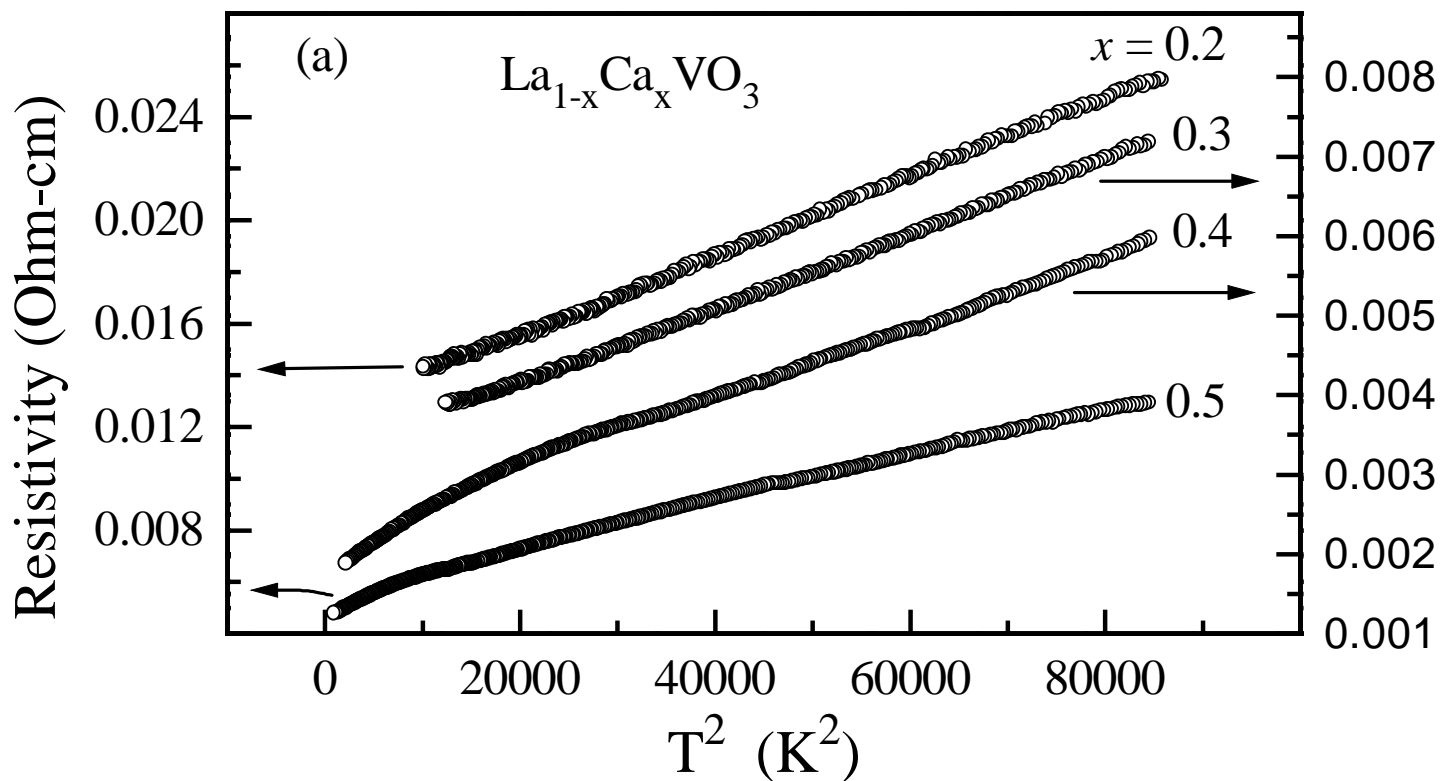
Maiti *et al.*, Fig. 1

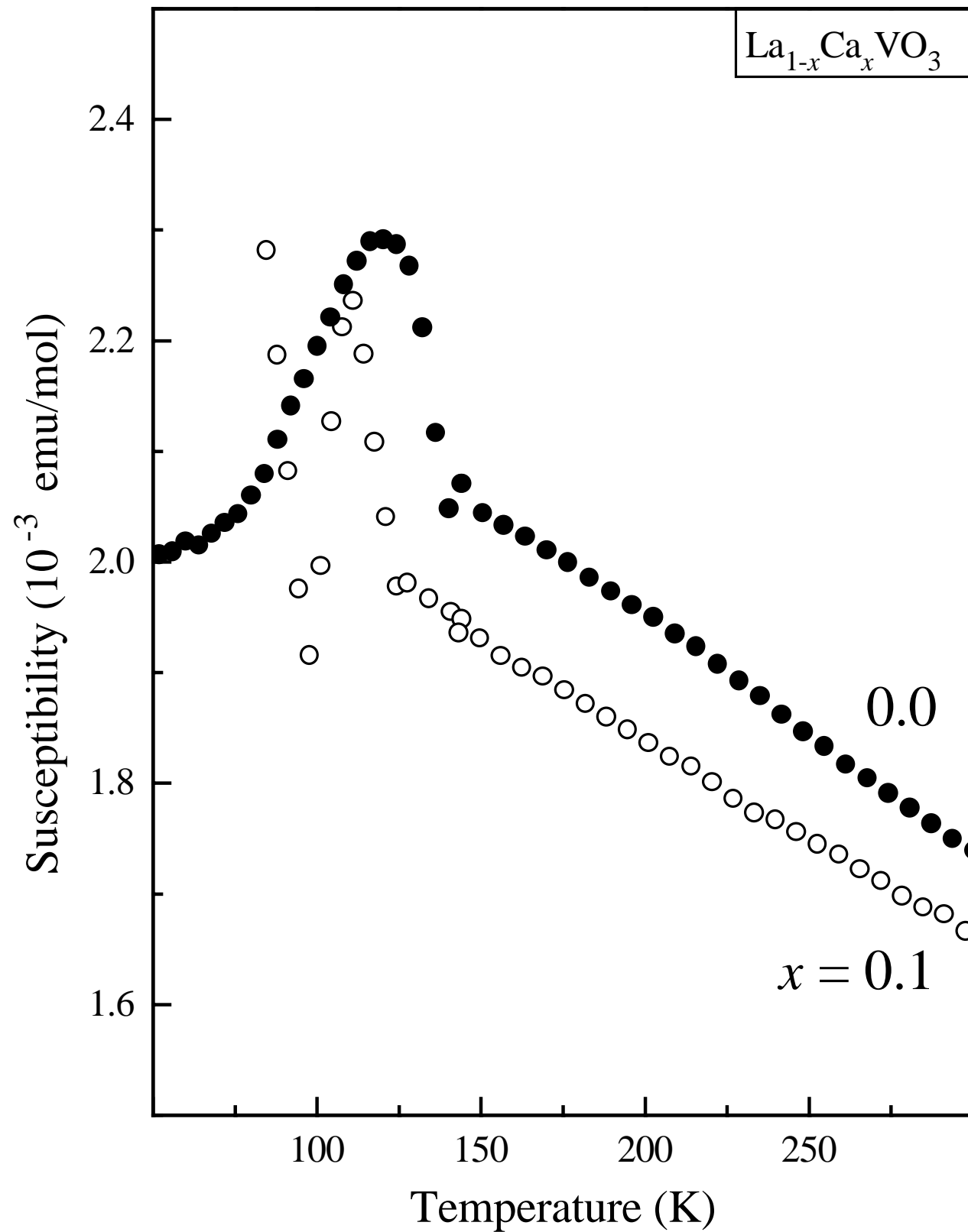


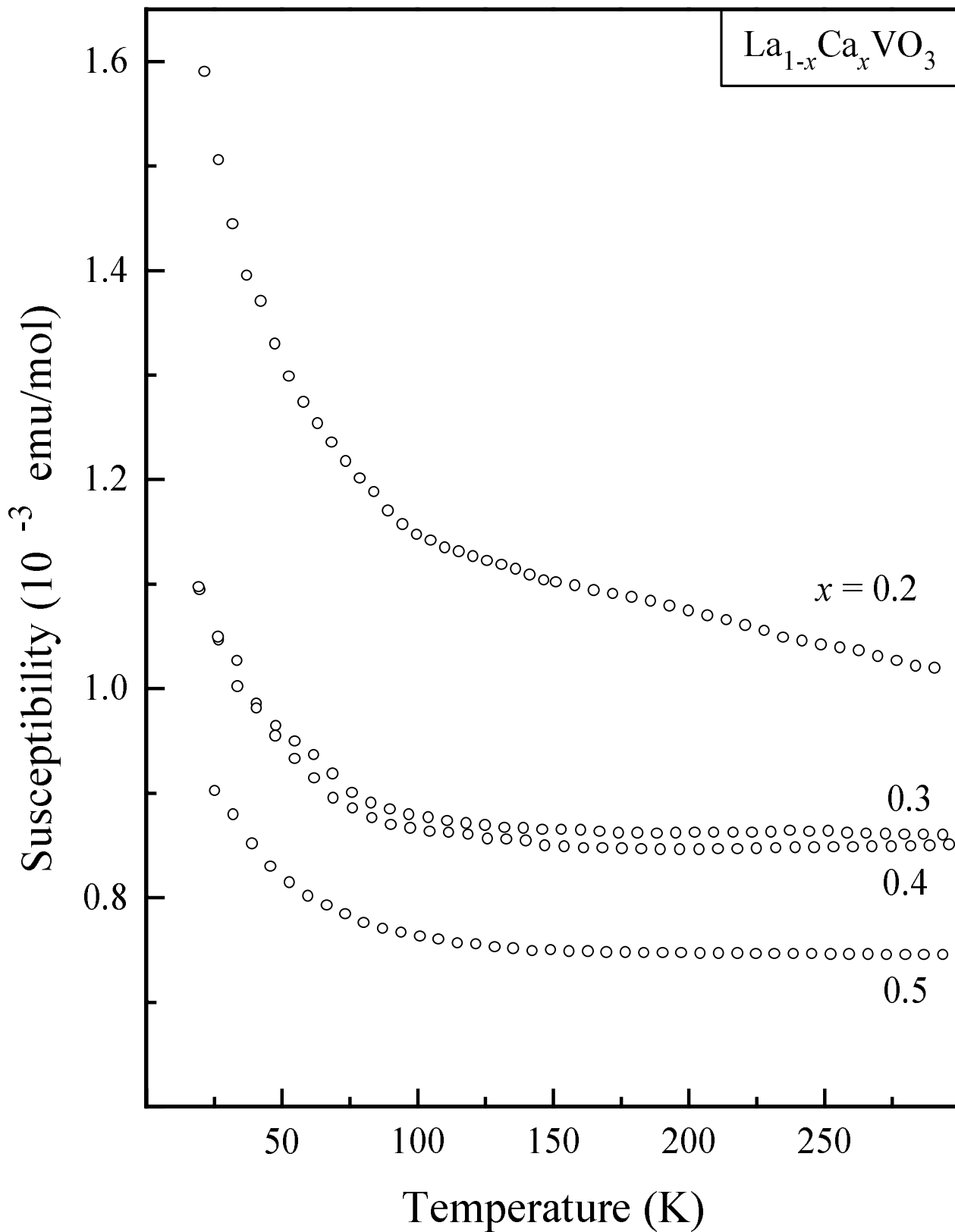
Maiti *et al.*, Fig. 2



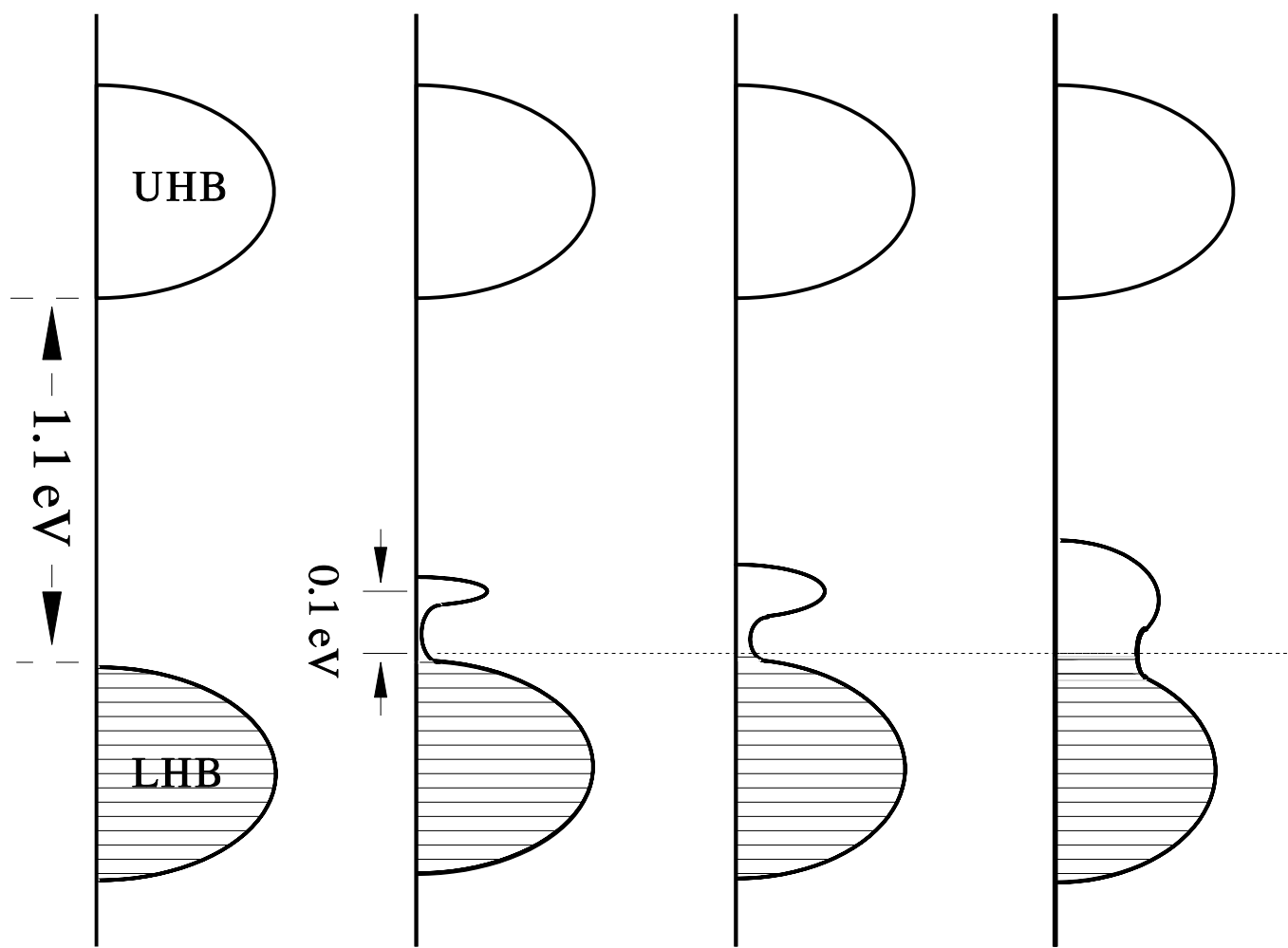
Maiti *et al.*, Fig. 3







Maiti *et al.*, Fig. 6



(a) LaVO_3

(b) $\text{LaVO}_{3+\delta}$

(c) $x < 0.2$

(d) $x \geq 0.2$

